Hybrid UAV with endurance and VTOL capabilities

Chung-How Poh, Chung-Kiak Poh

Hybrid UAV with endurance and VTOL capabilities

Chung-How Poh, and Chung-Kiak Poh

billyBun Aircraft, 23 Halaman York, 10450 Penang, Malaysia

Email address: billyBun.aircraft@gmail.com

Abstract

High-aspect ratio sailplanes are well known for their endurance while the unlimited aerobatic aircrafts are specially designed to perform maneuvers under stall conditions such as vertical hovering and the Lomcovák. We propose and simulate an UAV design based on the hybridization of sailplane and aerobatic aircraft. The aim is to design and develop an endurance UAV with VTOL (vertical take-off and landing) and payload capabilities.

1. Introduction

Two attributes of flying that capture the heart and soul of aviation enthusiasts are the ability to stay aloft for hours on a motorless glider and watching an Edge 540 aerobatic plane hanging mid-air entirely by its propeller thrust. In 2010, the Global Observer® by AeroVironment, Inc. successfully completed its maiden flight (AeroVironment, Inc. 2014). It has a wing span of 53.3 m and it was created as a persistence UAV (unmanned aerial vehicle) with endurance of 4 to 6 days, and operating altitude of 13.7 to 16.8 km (AeroVironment, Inc. 2014). Its payload capacity is 180 kg and it has an estimated wing loading of 235 $N \cdot m^{-2}$. Other examples of endurance UAV are the Phantom Eye by Boeing and the Ion Tiger developed by the U.S. Naval Research Laboratory (Boeing 2014; U.S. Naval Research Laboratory 2013). Important civilian and defense applications of endurance UAV include natural disaster management and monitoring, communications relay, weather

monitoring, GIS (geographic information system) mapping, maritime operations, and emergency aid delivery (Watts et al. 2012; AeroVironment, Inc. 2014).

The platform designs of endurance UAVs are generally based on sailplanes, which are fixed-wing aircrafts with very efficient wing and high glide ratio (Federal Aviation Administration 2011; Capata et al. 2014; Tuzcu et al. 2007). They are kept airborne by harnessing the energy of the atmosphere, primarily in the form of updrafts. A thermal updraft is a bubble or column of warm air that is rising and often a cumulus cloud will form at the top of the thermal, marking the area of lift (SoaringNV 2014). Thermal updrafts occur due to the convective process in the atmospheric boundary layer (Fisher et al. 2014). The average vertical velocity at an altitude z, within the thermal is given by (Fisher et al. 2014)

$$\overline{w} = w^* \left(\frac{z}{z_i}\right)^{1/3} \left(1 - 1.1\frac{z}{z_i}\right) \quad (1)$$

where w^* is the convective velocity scale, and z_i is the convective mixing layer thickness. Typical vertical velocity within the thermal is 2 to 5 ms^{-1} (Fisher et al. 2014), though values greater than 10 ms^{-1} have also been reported (Childress 2010). The other common type of updraft is orographic lift, where air is forced upwards by a slope such as hills or mountains (Whiteman 2000). Whenever the updraft is rising faster than the sink rate of a sailplane, there will be a gain of altitude. The rate of climb of a sailplane, V_c with its sink rate, V_s in an ascending thermal of average velocity, $\overline{w}$ is (Shannon 2002)

$$V_c = \overline{w} - V_s \quad (2)$$

While sailplanes are renowned for their endurance and high glide ratio, the hallmarks of aerobatic airplanes are their large control surfaces and power-to-weight ratio that exceeds unity which enable them to perform “3D maneuvers” such as hovering, inverted harrier, waterfall and blender (Zivko Aeronautics Inc. 2005; Extra Aircraft 2014; Fédération Aéronautique Internationale 2014).

Similar to sailplanes, endurance UAVs often require runway to take-off and land. However, suitable runway may not be available in situations such as in the aftermath of a hurricane, in hilly regions, or on board a ship. VTOL and hovering capabilities will, therefore, add greater flexibility to endurance UAVs, in that, they will be able to take-off and land virtually anywhere, as well as flying at much slower than their stall speeds, if required. Herein we propose the design of a hybrid UAV capable of both endurance and VTOL. The design involves the hybridization of sailplane and unlimited aerobatic aircraft. Flight simulation is used to demonstrate the VTOL capability and to evaluate flight performance including effect of payload.

2. Simulation details

Fig. 1 The as-supplied simulation sailplane Spirit 100

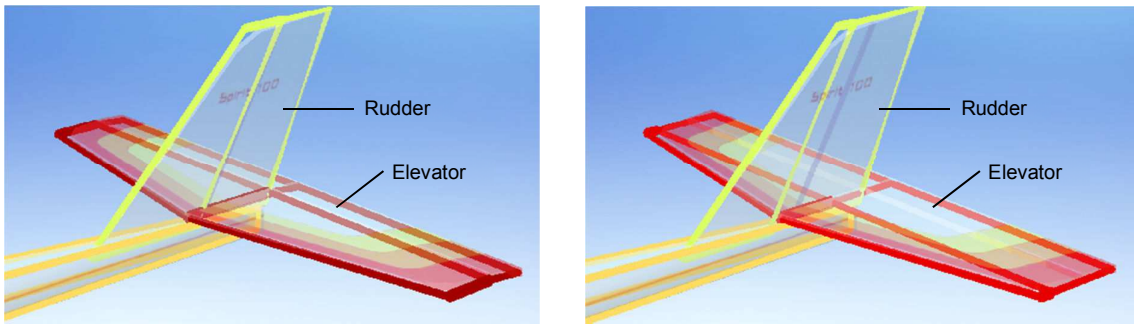

(a) (b)

Fig. 2 Comparison of rudder and elevator control surfaces on the (a) Spirit 100 and (b) Hybrid UAV.

Simulation work was performed using the RealFlight® 6.5 simulator (Great Planes® Model Mfg. 2014) running on a quad-core 2.2 GHz computer. The as-supplied simulation sailplane Spirit 100 with highly-efficient Selig 703 airfoil, as shown in Fig. 1, was used as the base platform to create the hybrid UAV. The motorless sailplane has a wing span of 2.53 m and flying weight of 1.7 kg. Modification of the Spirit 100 was done using the Accu-Model™ aircraft editor. Surface areas of the rudder and elevator were increased by adjusting the chord ratios, and the flaps were replaced by a pair of ailerons. Control surface areas of the original Spirit 100 and the hybrid UAV are as shown in Fig 2(a) and (b), respectively. The following components were added to the platform to enable powered flight: A 2204 W brushless motor with 121.72 N thrust, a pair of co-axial counter-rotating folding propellers (size: 432 x 174 mm), and a 6-cell 8000 mAh lithium polymer (Li-po) battery pack. Counter-rotating propellers have recently been employed in the prestigious FAI (Fédération Aéronautique Internationale) World Championship for Aerobatic Model Aircraft, class F3A (radio-control aerobatics) with positive results (Michael Ramel 2013). Angular position dependent 3-axis (roll, pitch, yaw) gyro was added to the platform for enhanced flight stability. The completed model weighed in at 3.085 kg. Various phases of flight and atmospheric conditions such as thermal updraft were simulated to evaluate the flight performance and capability.

Gliding performance was characterized using the polar curve, with the motor turned off and the propellers folded. The flight power was acquired by setting the sailplane on a straight and level flight, adjust the throttle until the desired airspeed is reached with the variometer showing zero readout; if the airspeed, altitude and electrical power value remained invariant for 1 minute, equilibrium conditions were considered reached and the power value was recorded as the power requirement. Effect of payload on flight performance was also evaluated at 1, 3, 5, and 7 kg. The center of mass of the aircraft was made to coincide with the center of lift throughout the simulation to ensure flight characteristics were not adversely affected.

3. Results and discussion

3.1. VTOL capabilities

Normal flight and VTOL capabilities were successfully demonstrated with good control over the roll, pitch and yaw, even with the payload of 7 kg. The use of the counter-rotating propellers was essential as it reduced the propeller torque effect and the P-factor to an almost negligible level, and consequently, virtually no aileron deflection was needed to maintain roll-free vertical hovering. This allowed for smaller ailerons to be used, symmetrical roll-rate on both directions, and improved the hovering stability. Less aileron deflection also resulted in greater vertical acceleration, which can be used to lift heavier payload.

Figs. 3(a) to (f) show the vertical landing sequence for the hybrid sailplane with 7 kg payload onboard. The landing sequence begun with the final approach and followed by the vertical climb and reduction in airspeed. As the nose pitched upward, the motor thrust was gradually increased until the platform came to a transition hovering (variometer showing 0 ms^{-1}). The platform was then brought into a constant rate of descent (-0.9 ms^{-1}, in this case) and terminated with the final hovering. Optionally, the platform could be steered with precision onto a landing station, if necessary [Fig. 3(f)].

Fig. 4 shows the hovering power for payload ranging from 0 to 7 kg, and a linear fit has been applied to the plot with a R^2 value of 0.9982. The 3.085 kg platform itself consumed 343.68 W for hovering and linear fitting gave 234.0 W kg^{-1} for any addition of payload.

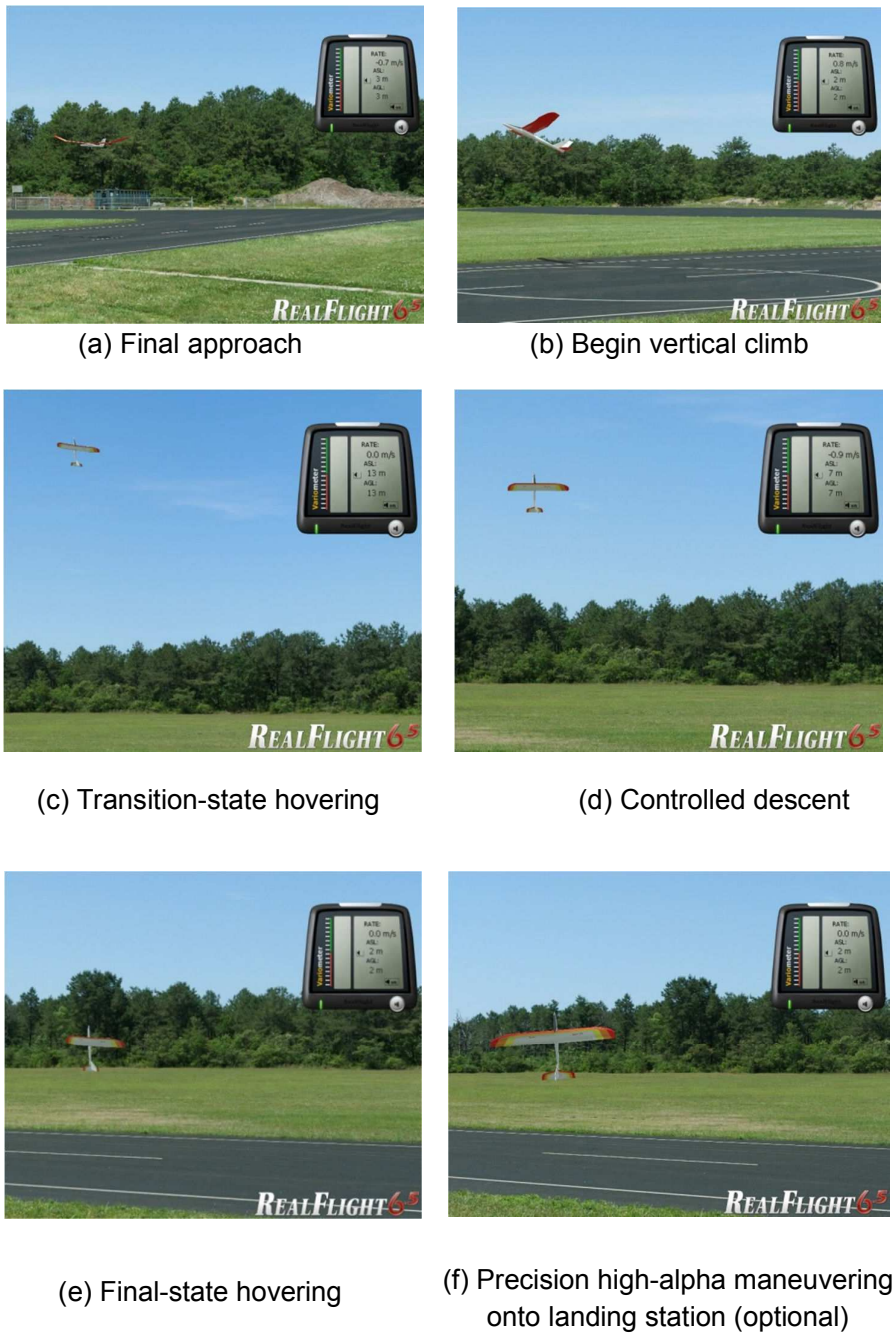

(a) Final approach (b) Begin vertical climb

(c) Transition-state hovering (d) Controlled descent

(e) Final-state hovering (f) Precision high-alpha maneuvering onto landing station (optional)

Fig. 3 Vertical landing sequence

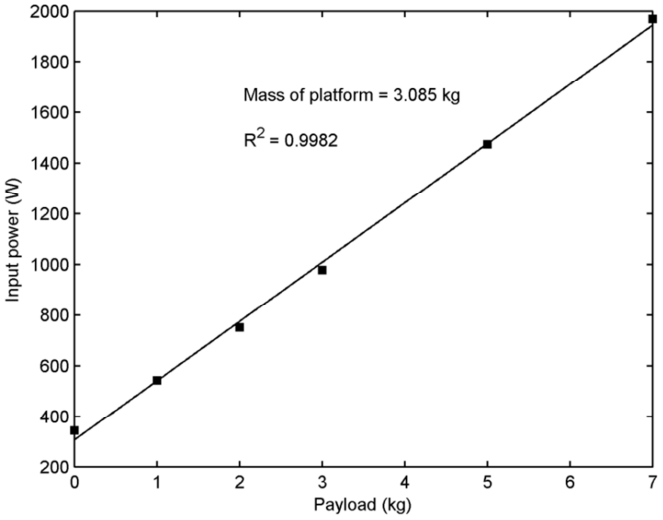

Fig. 4 Hovering power as a function of payload.

3.2 Gliding performance

Gliding performance of the hybrid sailplane with varying payloads was evaluated using the polar curves, as shown in Fig. 5, from which minimum sink rates and maximum glide ratios were obtained. The glide ratio refers to how far a glider can travel for a given altitude. A line is drawn from the origin tangent to the polar curve, and the speed indicated by the point of tangency is the speed to achieve maximum glide ratio (Holtz 2012). The minimum sink rate is the speed at which the glider is descending at a slowest possible rate through the air (Holtz 2012). Table 1 summarizes the maximum glide ratio and the minimum sink rate for different payloads, along with other crucial parameters such as the flying weights and wing loadings. It is interesting to note that despite relatively large difference in the payload, the minimum sink rate only varied between 0.6 and 1.0 ms^{-1}.

The stall speed was derived from Fig. 5 as well. Additionally, the platform with 7 kg payload was simulated with a pair of unfolding propellers, and as expected, the wind-milling propeller drag degraded the minimum sink rate significantly and resulted in a maximum glide ratio of

only 7.3. The platform is denoted as “Hybrid (7 kg, prop)” in Table 1. This re-enforced the fact that folding propeller is essential to the endurance and gliding performance of sailplanes.

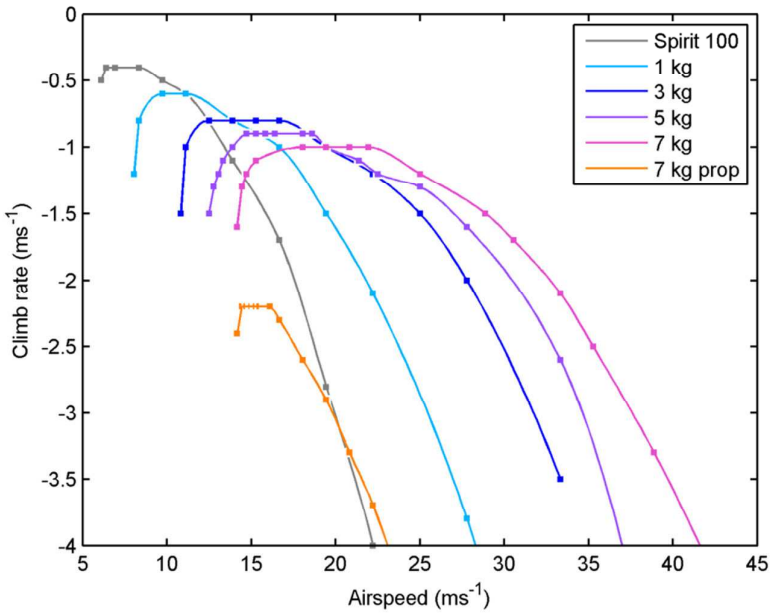

Fig. 5 Polar for the original Spirit 100 and the hybrid sailplane with different payloads. “Prop” indicates the platform with unfolding propeller.

Table 1 Key flight parameters for the simulated hybrid sailplane of various configurations.

Configuration of platform	Flying weight (kg)	Wing loading ($N \cdot m^{-2}$)	Hovering input power (W)	Stall speed ($km \cdot h^{-1}$)	Minimum sink rate (ms^{-1})	Best glide speed ($km \cdot h^{-1}$)	Maximum glide ratio
Spirit 100	1.745	25.27	N/a	22	0.4	31	21.1
Hybrid (0 kg)	3.085	44.67	343.68	28	0.6	42	19.7
Hybrid (1 kg)	4.085	59.14	542.82	29	0.7	42	19.0
Hybrid (3 kg)	6.085	88.10	978.80	39	0.8	62	21.1
Hybrid (5 kg)	8.085	117.06	1474.86	49	0.9	67	20.7
Hybrid (7 kg)	10.085	146.02	1968.44	50	1.0	81	22.2
Hybrid (7 kg, prop)	10.085	146.02	1968.44	51	2.2	59	7.3

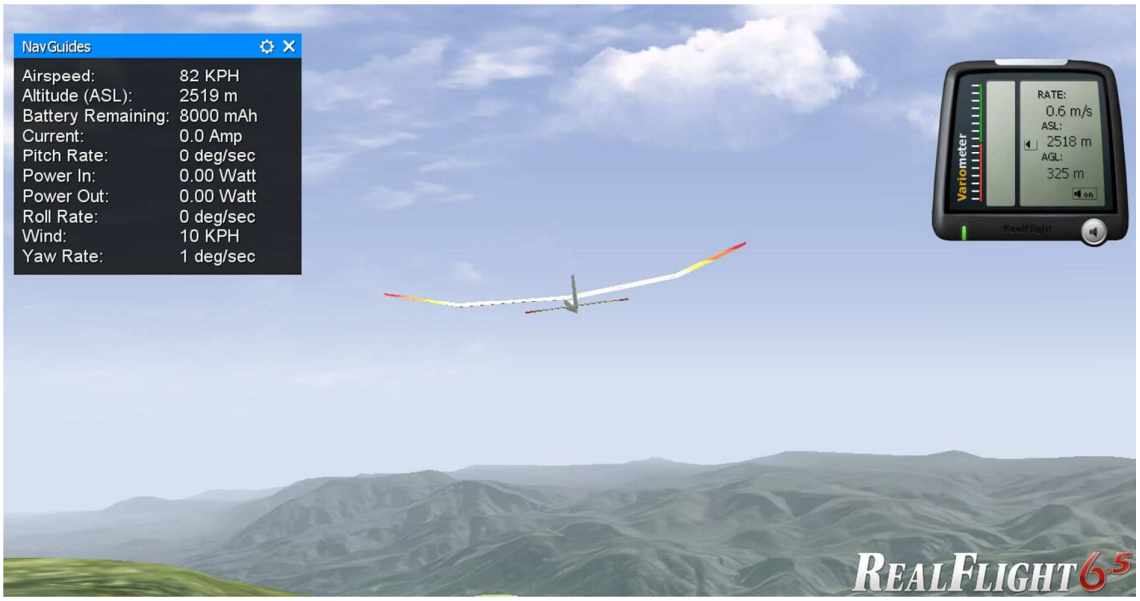

Fig. 6 Slope glide testing with horizontal wind speed of 10 kmh^{-1} for the hybrid sailplane carrying 7 kg payload.

Sink rates (V_s) of 0.6 to 1 ms^{-1} found in this simulation study implied that average thermal velocity ($\overline{w}$) of 1 ms^{-1} or more is sufficient to keep the platform airborne, as indicated by Eq. 2. Obviously the thermalling conditions will be more easily fulfilled with the lighter payloads. Slope gliding test was simulated to evaluate the gliding performance of the platform with 7 kg payload. It was found that horizontal wind speed of 10 kmh^{-1} was able to produce a climb rate (V_c) of 0.6 m/s, as shown by the variometer in Fig 6. Climb rate as high as 3.6 ms^{-1} has been observed close to the slope in 21 kmh^{-1} wind. No propulsion was necessary in this flight test and so the battery capacity remained at 8000 mAh.

3.3 Power-assisted flight

This section focuses on assessing the power-assisted flight when insufficient thermal is available. In this scenario, the lift contribution comes from the propulsion system of the aircraft and the rising thermal. The stronger the thermal, the less input power is needed to stay aloft. Fig. 7(a) shows a plot of electrical power consumption as a function of sink rate for various payloads. 7000 mAh of the battery capacity was used to calculate the endurance

and the remaining 1000 mAh was reserved for VTOL, plus a margin of safety. The endurance flight time was computed solely based on electrical current drawn, and any additional flight time gained from power-off gliding was neglected. The flight time achievable with different sink rate is as shown in Fig. 7(b). The endurance curves for 1 and 3 kg payload are of particular relevant to monitoring and surveillance applications as many of the recently developed onboard devices for small UAVs tend to fall within this range. Among them are the compact and light-weight YellowScan LiDAR system developed by L'Avion Jaune (L'Avion Jaune 2012), and the 90 g multi-spectral imaging system by Tetracam Inc. (Tetracam Inc 2011). In the complete absence of thermal, the platform with 1 and 3 kg payloads were able to stay airborne ($V_s = 0$ ms^{-1}) for 1.64 and 1.05 hours, respectively. $\overline{w}$ < 200 ft min^{-1} (1.016 ms^{-1}) is regarded as weak thermal (U.S. National Weather Service 2014). Fig. 8 shows the duration of the power-assisted flight as a function of the payload in presence of weak thermal of $\overline{w}$ = 0.5 ms^{-1}. Sink rate V_s, was set to 0.4 ms^{-1} to obtain an overall climb rate V_c, of 0.1 ms^{-1} (Eq. 2). The positive climb rate may also be used to gain forward speed (kinetic energy). Under these conditions, the platforms with 1 and 3 kg payloads were predicted to have flight times of 2.14 and 1.36 hours, respectively.

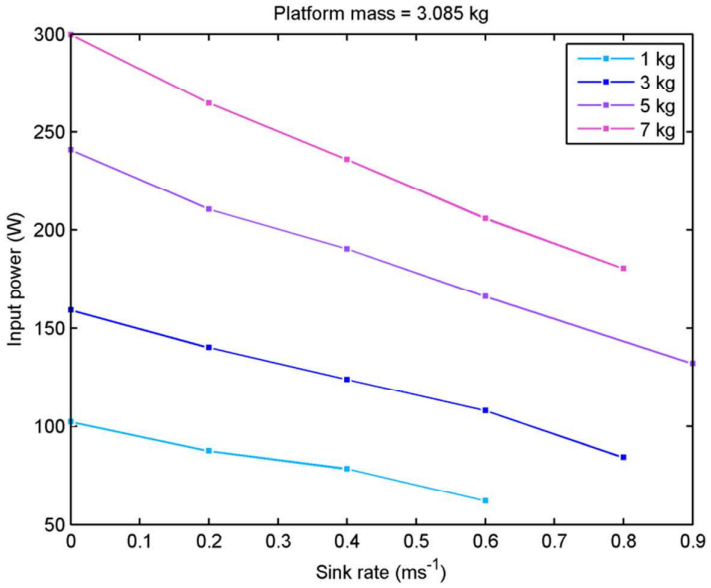

(a)

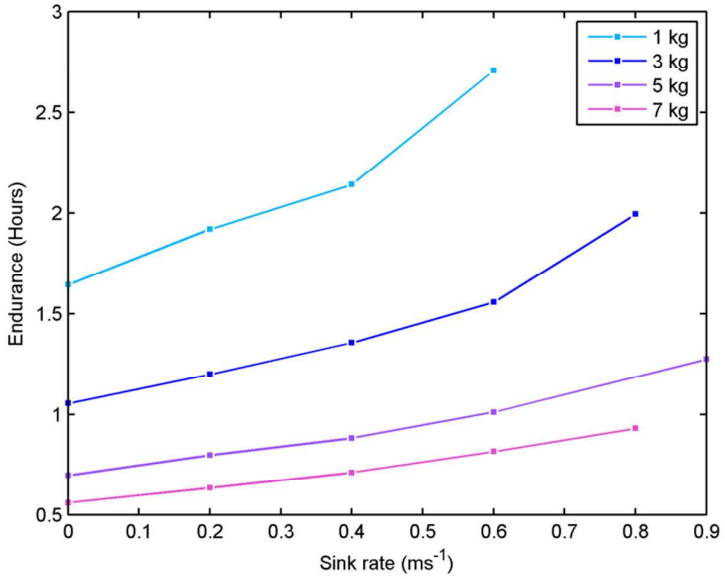

(b)

Fig. 7 Sink rate and the corresponding (a) input power and (b) flight endurance for different payloads.

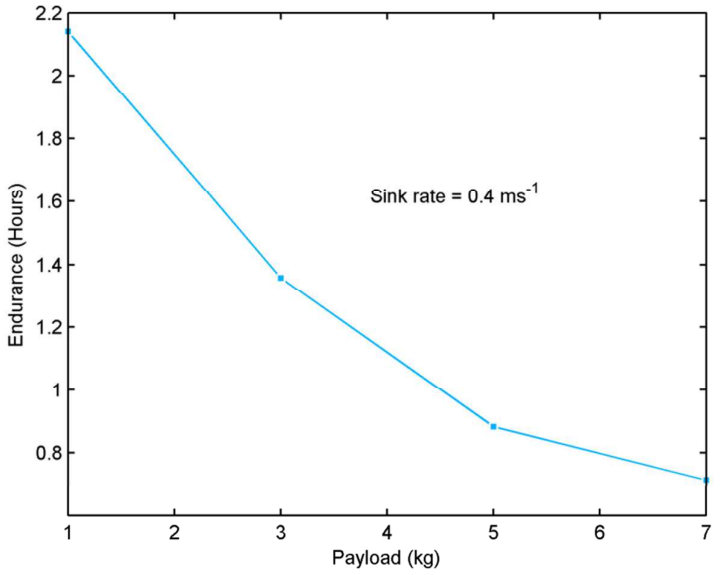

Fig. 8 Flight times predicted for power-assisted flight in weak thermals ($\overline{w}$ = 0.5 ms^{-1}) with a climb rate, V_c of 0.1 ms^{-1}.

The endurance and payload capacity may be further extended by applying the concept of hybridization and VTOL capability proposed in this work to larger platforms, as they tend to be more efficient, despite having a significantly higher wing loading. For example, the full-sized FAI-class 18-meter ASG 29 sailplane has a maximum glide ratio of 52:1 and a minimum sink rate of 0.47 ms^{-1} (Alexander Schleicher GmbH & Co 2014). Furthermore, its payload capacity is 320 kg. The wing loading is 323.6 to 560.0 $N{\cdot}m^{-2}$, versus 146.02 $N{\cdot}m^{-2}$ for the hybrid UAV platform with 7 kg payload simulated in this work. From the aspect of propulsion system, endurance can be improved by the use of liquid hydrogen fuel as demonstrated by the Global Observer or the Ion Tiger. Lightweight flexible solar cell with conversion efficiency of approximately 25% will certainly be a candidate as well.

VTOL-endurance UAV is envisioned to have important applications. For example, they can be deployed quickly in a multi-agent system to support first responders in disaster scenarios by providing services such as high resolution aerial imagery and communications relay.

Conclusions

We have proposed and simulated a hybrid sailplane UAV with VTOL and payload capabilities. The simulated platform was found to have stable and predictable flight characteristics during cruising and gliding. It demonstrated controllable vertical descent with a descent rate of up to 2 ms^{-1} and with 7 kg payload. The use of single-axial counter-rotating propellers greatly enhanced the hovering stability and enabled symmetrical roll-rate on both directions. The VTOL feature is particularly useful when proper runway is not available, such as in hilly regions or on board sea vessels. Future work will involve prototyping the platform.

References

AeroVironment, Inc. 2014. Global Observer®. Available from http://www.avinc.com/globalobserver/ [accessed August 2014].

Boeing. 2014. Phantom Eye. Available from http://www.boeing.com/boeing/bds/phantom_works/phantom_eye.page [accessed April 2014].

U.S. Naval Research Laboratory. 2013. NRL Shatters Endurance Record for Small Electric UAV. Available from http://www.nrl.navy.mil/media/news-releases/2013/nrl-shatters-endurance-record-for-small-electric-uav [accessed August 2014].

Watts, A.C., Ambrosia V.G., and Hinkley E.A. 2012. Unmanned Aircraft Systems in Remote Sensing and Scientific Research: Classification and Considerations of Use. Remote Sens. **4**(6):1671–1692.

Federal Aviation Administration. 2011. Glider Flying Handbook. Skyhorse Publishing, New York, USA.

Capata, R., Marino, L., and Sciubba, E. 2014. A hybrid propulsion system for a high-endurance UAV: configuration selection, aerodynamic study, and gas turbine bench tests. J. Unmanned Veh. Sys. **2**(1): 16–35. doi: 10.1139/juvs-2013-0005

Tuzcu, I., Marzocca, P., Cestino, E., Romeo, G., and Frulla, G. 2007. Stability and Control of a High-Altitude, Long-Endurance UAV. J. Guid. Control Dynam. **30**(3): 713–721. doi: 10.2514/1.25814

SoaringNV. 2014. What is soaring? – lift. Available from http://www.soaringnv.com/index.php?page=2 [accessed August 2014].

Fisher, E., Tubul, M., and Shemesh, I. 2014. Collecting Wind Energy Using Thermal Updrafts. International Conference on Renewable Energies and Power Quality (ICREPQ'14), Cordoba (Spain).

Childress, C.E. An empirical model of thermal updrafts using data obtained from a manned glider. 2010. M.Sc. Thesis. University of Tennessee.

Whiteman, C.D. 2000. Mountain meteorology: fundamentals and applications. Oxford University Press, New York, USA.

Shannon, H.D., Young, G.S., Yates, M.A., Fuller, M.R., Seegar, W.S. 2002. Measurements of thermal updraft intensity over complex terrain using American white pelicans and a simple boundary-layer forecast model. Bound.-Layer Meteor. **104**(2): 167–199.

Zivko Aeronautics Inc. 2005. Edge Aircraft. Available from http://www.zivko.com/edge/site.html [accessed April 2014].

Extra Aircraft. 2014. Extra aerobatic aircrafts. Available from http://www.extraaircraft.com/aircraft.php [accessed April 2014].

Fédération Aéronautique Internationale. 2014. Powered aerobatics. Available from http://www.fai.org/civa-our-sport/powered-aerobatics [accessed April 2014].

Great Planes® Model Mfg. 2014. RealFlight® radio control flight simulator. Available from http://www.realflight.com/ [accessed April 2014].

Ramel, M. 2013. Coaxial Drive Propulsion for F3A Models. Available from http://www.sebart.it/img-F3A/coaxial-drive/coaxial-drive-description.html [accessed April 2014].

Holtz, R. 2012. Glider Pilot's Handbook of Aeronautical Knowledge. White Oak Communications, North Carolina, USA.

L'Avion Jaune. 2012. YellowScan Ultra-light laser scanner system. Available from http://yellowscan.lavionjaune.com/ [accessed April 2014].

Tetracam Inc. 2011. Tetracam Multi-spectral Imaging Systems Overview. Available from http://www.tetracam.com/Products1.htm [accessed April 2014].

U.S. National Weather Service. 2014. Soaring Guidance. Available from http://forecast.weather.gov/product.php?site=BOU&product=SRG&issuedby=BOU [accessed April 2014].

Alexander Schleicher GmbH & Co. 2014. ASG 29. Available from http://www.alexander-schleicher.de/produkte/asg29/asg29_main_e.htm [accessed August 2014].